Chinese Chemical Letters 34 (2023) 107940

Contents lists available at ScienceDirect

Chinese Chemical Letters

journal homepage: www.elsevier.com/locate/cclet

Tactfully revealing the working mechanisms on a tetraarylimidazole derivative: AIE characteristic, ESIPT process and ICT effect integrating in one molecule

Min Liu[a,b,c], Shibo Zhong[a], Bin Feng[a], Yueming Ren[a], Xiaohui Liu[a], Shuaige Bai[a], Fei Chen[a], Shao Liu[b,c], Wenbin Zeng[a,*]

[a] Xiangya School of Pharmaceutical Sciences, Central South University, Changsha 410013, China
[b] Department of Pharmacy, Xiangya Hospital, Central South University, Changsha 410008, China
[c] National Clinical Research Center for Geriatric Disorders, Xiangya Hospital, Central South University, Changsha 410008, China

ARTICLE INFO

Article history:
Received 11 September 2022
Revised 10 October 2022
Accepted 24 October 2022
Available online 1 November 2022

Keywords:
Tetraarylimidazole derivative
Aggregation-induced emission
Excited-state intramolecular proton transfer
Intramolecular charge transfer
Density functional theory
Time-dependent density functional theory

ABSTRACT

Recently, a novel tetraarylimidazole derivative 2-(benzo[d]thiazol-2-yl)-4-(4,5-bis(4-methoxyphenyl)-1-phenyl-1*H*-imidazol-2-yl)-phenol (be called MHBT herein) was architectured by our research group showing the fascinating synergy of aggregation-induced emission (AIE) characteristic, excited-state intramolecular proton transfer (ESIPT) mechanism and intramolecular charge transfer (ICT) effect. Nevertheless, a detailed and reasonable interpretation of its mechanisms both in theory is urgently needed. Consequently, to unveil the working mechanism meticulously, herein, we tactfully applied density functional theory (DFT) and time-dependent density functional theory (TD-DFT) methods to illuminate the underlying mechanisms in different solvent conditions. After optimizing the structures, the geometric parameters of hydrogen bonds (HBs), the infrared (IR) vibrational spectrum, the reduced density gradient (RDG) isosurfaces were calculated in detail, vividly explaining how the enhancement of HBs behaved as the driving force to proceed ESIPT process. Simultaneously, the frontier molecular orbitals (FMOs) combined with the potential energy curves (PECs) were conducted to interpretate the role and character of ICT and ESIPT in molecule MHBT. Further, the PECs of MHBT for dihedral angles in different organic solvents were calculated to compare the dominant torsion degree, rationalizing the AIE phenomenon from the view of the restriction of intramolecular rotation process. This work may well underpin the understanding of the interaction between different mechanisms in fluorescent dyes and thereby provide meaningful guideline for the design and construction of ideal molecules

Fluorescent molecular probes have drawn widespread attention for chemical sensing and optical imaging owing to the unique merits, such as high selectivity, remarkable sensitivity, ultrafast response time, convenient to handle and real-time, nondestructive visual detection [1–3]. Generally, the fluorescence properties of fluorescent probes need be fine-tuned for specific applications [4–6]. Given this, comprehensive understanding of the used fluorophores and their fluorescent mechanisms are vital for the development and construction of an optimal fluorescent probe. Up to now, several fluorescence signaling mechanisms have been proposed and utilized in the design of probes, including the aggregate induced emission (AIE), the excited state intramolecular proton transfer (ESIPT), the intramolecular charger transfer (ICT), the photo-induced electron transfer (PET), the föster resonance energy transfer (FRET) and so forth (Scheme 1). Among them, ESIPT is a process featured by the proton migration within an intramolecular neighboring hydrogen-bonding site, in which occurs a photo-induced proton tautomerization from enol form to keto form giving rise to large Stokes shifts (Scheme 1b) [7]. In recent year, many efforts have been devoted to study this effect because the tautomerization in ESIPT usually leads to rapid photo-induced proton transfer and thus cause substantial changes in the fluorescence spectra [8–10]. Meanwhile, the mechanism action of ICT is characterized by the electron delocalization and transfer in a single molecule to generate a "push-pull" π electron system in the excited state [11]. And these fluorescent molecules based on ICT have been utilized for the imaging of analytes of interest *via* regulating the ICT strength, generally exhibiting an apparent hypsochromic

* Corresponding author.
E-mail address: wbzeng@hotmail.com (W. Zeng).

https://doi.org/10.1016/j.cclet.2022.107940
1001-8417/

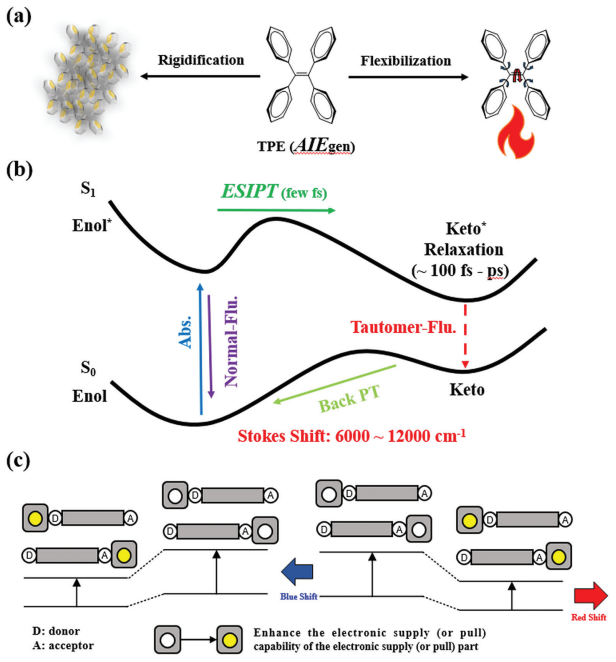

Scheme 1. The graphic illustrations to vividly portray the (a) AIE, (b) ESIPT and (c) ICT mechanism, respectively.

or bathochromic shift in the absorption/fluorescence spectrum (Scheme 1c) [12–14]. Additionally, AIE refers to the unique phenomenon that some fluorophores show significantly boosted fluorescence in aggregated state but faint fluorescence in the molecularly dissolved state (Scheme 1a) [15–17]. In particularly, AIE-based probes could present obvious fluorescence changes upon analytes-triggered solubility decreases, with advantages of signal amplification and low background noises. Nevertheless, a "turn-on" mode is generally exhibited. By contrast, the ESIPT and ICT-based fluorescent probes classically manifest the ratiometric mode in fluorescence sensing which gain an edge on the little background, minimized interference from instrumental factors and the concentration of probe, and other analyte-independent factors. Hence, it is of great significance to explore the potential tunability of ESIPT and/or ICT in AIE molecules and make these mechanisms manifest synergic effects in one fluorescent probes.

Imidazole, known as a typical asymmetric five-member heterocyclic ring [18], has received substantial attentions in multiple fields, such as photoelectricity [19], catalysis [20], drug synthesis [21] and so forth. Particularly, the derivatives of imidazole compounds are increasingly being used as a basic building block in the photoelectric area, from organic light emitting diode (OLED) [22], non-linear photonics [23] to mechanoluminescence [24]. This is mainly ascribed to the distinguished photoelectricity nature of the imidazole core, for example, excellent quantum yield or efficiency [25,26], photostability [27], balanced charge mobility [28]. Lately, our group found obvious AIE phenomenon in tetraarylimidazole, and based on it, elaborately developed a variety of tetraarylimidazole derivatives as the signal components for detection and imaging of various biologically relevant species or events, such as gram-positively bacteria [29], mercury ion [30], disease-associated proteins [31], cancer cell nucleus [32] and gas signaling molecules like carbon monoxide [33]. Unfortunately, these AIE probes typically exhibit "turn-on" mode and therefore suffer from analyte-independent interferences due to the lack of an internal standard. To address this dilemma, a 2-(2′-hydroxyphenyl) benzothiazole (HBT) moiety was introduced to the tetraarylimidazole core and a novel fluorophore 2-(benzo[*d*]thiazol-2-yl)-4-(4,5-bis-(4-methoxyphenyl)-1-phenyl-1*H*-imidazol-2-yl) phenol, referred to as MHBT (Fig. S1 in Supporting information), was developed allowing ratiometric responding behavior [33]. Interestingly, we found that it has some unique photophysical chemical phenomena, with the synergistic and collaborative actions of AIE, ESIPT and ICT effects. With perspective of the structural feature, a classic ESIPT unit hydroxyphenyl-benzothiazole (HBT) was coupled with the AIE-active tetraarylimidazole-based fluorophore. Further, the methoxy group, conjugation system, and even hydroxyl group in MHBT unit will also contribute to the ICT effect. Such a unique structure provides opportunities for understanding how these three characteristics works in a single molecular system. Indeed, the coexistence and synergistic effect of these characteristics were observed in the investigation of solvatochromism. To unveil its working mechanism and underpin our understanding toward such ratiometric AIE probes, it is highly desirable to carry out detailed research.

In this theoretical work, the underlying fluorescence mechanisms of molecule MHBT, including ESIPT, ICT and AIE, were revealed through DFT and TD-DFT methods in different solvent environments. The geometric parameters of the HBs, the IR vibrational spectra, RDG isosurfaces and scatter plots, were taken to elucidate the impact of solvents on the hydrogen bonding strength. The abilities of key functional group (-OH) for the proton (H) acceptor and donor, and subsequently the charge transfer (CT) process of molecule MHBT were investigated as well by the analysis of the FMOs in this work. Similar results of dominant ESIPT process were confirmed in the located transition state (TS) and evaluated by the PECs. Further, the involving TS and the reaction energy in four different kinds of solvent environments were also calculated to assess the impact of ICT on the fluorescence characteristics. The evaluation of torsion degree in molecular conformation and the analysis of PECS toward dihedral angles demonstrate that the AIE activity of molecule MHBT, to a great degree, can be ascribed to the constraint of intramolecular rotation (RIR) process. Expectantly, this paper may facilitate our understanding of the comprehensive role of different mechanisms in fluorescent dyes as well as construction of organic chromophores with better photophysical chemistry properties.

The optimized compound geometry of molecule MHBT based on PBE0/6-31G(d, p) in four different kinds of organic solvents with different dielectric constants (DMSO, ACN, DCM and DIO), including the normal and tautomeric structures of MHBT in the S_0 and S_1 states, are exhibited in Figs. S1a and b. The HBs occurring sites in the normal and tautomeric structures in Fig. S1 are annotated in number of O1-H2···N3 and O1···H2-N3, respectively. To make a more intuitive comparison, the lengths of hydrogen bond and their angles are formulated in Table S2 (Supporting information). It can be found in Table S2, from the S_0 to S_1 states, the length of intramolecular hydrogen bond for H2··O1 rose by 0.02142 Å (DMSO) < 0.02146 Å (ACN) < 0.02222 Å (DCM) < 0.02414 Å (DIO), and the O1-H2-N3 bond angle grown-up by 4.248° (DMSO) < 4.251° (ACN) < 4.252° (DCM) <4.253° (DIO), respectively. Apparently, these results certified that the intramolecular hydrogen bond in molecule MHBT is intensified from the S_0 to S_1 state regardless of the solvent in which they are present, which is more favorable for proton transfer happens in S_1 state. More importantly, the order of bond length for H2···N3 in the S_1 state displays in the following way: DMSO (1.59592 Å) > ACN (1.59583 Å) > DCM (1.59507 Å) > DIO (1.59398 Å) and the corresponding order of bond angles for O1-H2-N3 is presented as below: DMSO (152.475°) > ACN (152.473°) > DCM (152.453°) > DIO (152.318°). Hence, these calculation results certified that the hydrogen bond strength in different organic solvents according in follow sequence: DMSO < ACN < DCM < DIO, which is in accord with the observed orders of the ESIPT occurrence. In other words, this

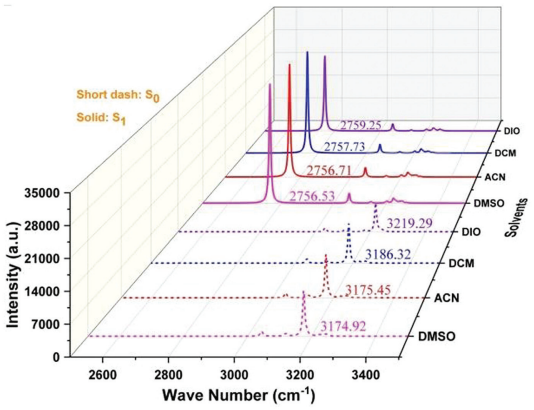

Fig. 1. The calculate values of IR vibrational spectra for the hydrogen bond O1···H2 of molecule MHBT on the S_0 and S_1 states under four solvent (DMSO-ACN-DCM-DIO) environments based on PBE0/6-31G(d, p) levels.

demonstrated that the intramolecular hydrogen bond interaction gradually increased when the dielectric constant decreases.

After optimizing the structure, IR vibration frequency spectra analysis was implemented to evaluate the impact of solvents environment toward the strength of hydrogen bond [34,35]. As presented in Fig. 1, the IR vibration spectrum of O1-H2 are 3174.92 cm^{-1} (DMSO), 3175.45 cm^{-1} (ACN), 3186.32 cm^{-1} (DCM), 3219.29 cm^{-1} (DIO) separately, then upon photo-excitation, the IR stretching vibration frequencies of O1-H2 in the S_1 state turn into 2756.53 cm^{-1} (DMSO), 2756.53 cm^{-1} (ACN), 2757.73 cm^{-1} (DCM), 2759.25 cm^{-1} (DIO), respectively. Through analysis, it can be found that the IR vibration frequency of intramolecular hydrogen bond O1-H2 exhibited a prominent bathochromic shift from the S_0 to S_1 state, proving the enhancement of the corresponding exhibited a prominent bathochromic shift from the S_0 to S_1 state, proving the enhancement of the corresponding intramolecular hydrogen bond for molecule MHBT in the S_1 state. More importantly, the IR vibration frequency shows the bathochromic shift as in same sequence in the S_0 state (DMSO: 418.39 cm^{-1} < ACN: 418.74 cm^{-1} < DCM: 430.59 cm^{-1} < DIO: 463.56 cm^{-1}) as well as in the S_1 state (DMSO: 2756.53 cm^{-1} < ACN: 2756.71 cm^{-1} < DCM: 2755.73 cm^{-1} < DIO: 2759.25 cm^{-1}) demonstrated that the intramolecular hydrogen bond intensifies more greatly while the dielectric constant of solvents decreases. Thus, the conclusion drawn from the IR vibration spectra analysis is in well agreement with that from the structural parameters, which helps further comprehend the ESIPT process.

As a rule, the RDG function is another way to study hydrogen bond, in which the calculated RDG isosurfaces could show and highlight the relationship between proton transfer and hydrogen bond intensity more intuitively. As depicted in Fig. 2a, the H-bond is painted as blue color, and the van der Waals forces is denoted as green to yellow color, while the repulsive forces is represented as yellow to red, for example steric hindrance. As seen in the screenshot, the bluer of the isosurface color, the HBs become stronger. As displayed in Fig. 2b, the color of the S_1 state gradient isosurface is distinctly darker than that of the S_0 state, suggesting that molecule MHBT in all the four solvents are enhanced under photoexcitation, which is consistent with the above calculated results. Simultaneously, in the scatter graphs of Figs. 2c and d and Fig. S2 (Supporting information), the spikes in the S_0 and S_1 states are at ($\rho \approx 0.04$ a.u.) and ($\rho \approx 0.05$ a.u.), respectively. Thus, the strength of the hydrogen bond in the S_1 state is stronger than that in the S_0 state. Such an enlargement of modulus of $sign((\lambda_2)\rho(r))$ demonstrates the conclusion again that the intramolecular hydrogen bond interaction become stronger upon excitation to S_1 state. Given these results, it was verified that the intramolecular hydrogen bonding is strengthened upon photoexcitation. Further, we accessed the impact of solvent environment on the strength of the intramolecular hydrogen bond as well. Similarly, the hydrogen bond intensifies as the decrease of solvents dielectric constant, manifesting more favorable occurrence of the ESIPT process.

With the addition of the above analysis, the CT process and redistribution procedure are accessed as the key indicators of proton transfer [36]. Firstly, we implemented the electron hole analysis and the molecular electrostatic potential (MEP) of molecule MHBT are shown in Figs. S1c–f. The H atom positive electrostatic potential as well as the hydroxyl O and N atom negative electrostatic potential reveals the susceptibility of hydrogen bond formed in O–H···N site for molecule MHBT in S_0 state. Upon photoexcitation, an apparent electron transfer occurs in S_1 state, suggesting the ICT process. Further, on account of the photoexcitation is generally accompanied with electron rearrangements, the behavior of FMOs for molecule MHBT to investigate the inherent relationship between ICT and ESIPT were analyzed as well. As presented in Table S3 (Supporting information), although the oscilla-

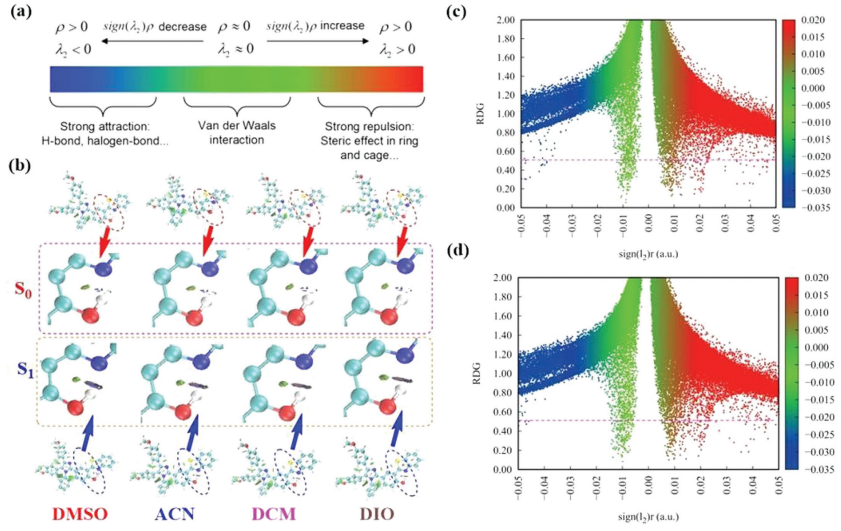

Fig. 2. (a) The color gradient axise and (b) visual diagram of the RDG isosurfaces for molecule MHBT in four kinds of solvents. (c, d) RDG(r) *versus* $\Omega(r)$ in S_0 and S_1 state of solvent DMSO.

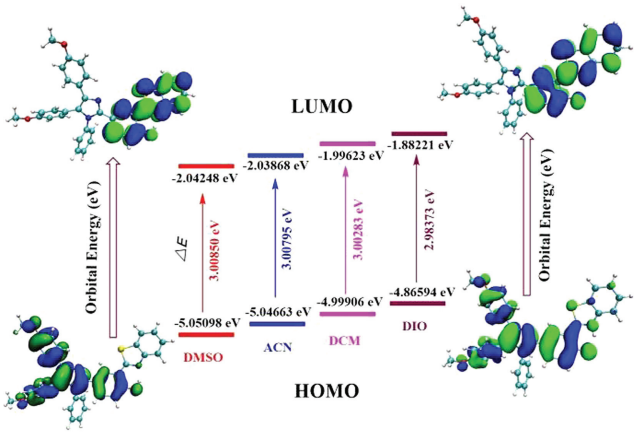

Fig. 3. The LUMO and HOMO of molecule MHBT in the S_1 state and the corresponding transition energies at the PBE0-D3/6-31G(d, p)/IEFPCM levels.

tor strength (*f*) of molecule MHBT in the S_2 state is greater than other states, the first singlet transition ($S_0 \rightarrow S_1$) is mainly located in highest occupied molecular orbital (HOMO) and lowest unoccupied molecular orbital (LUMO) due to the even greater orbital transition (OT) contributions to the electronic exited states (CI) than 98%. More importantly, the calculated wavelength of emission is generally identical to the experimental data what we got. The visualization patterns of FMOs from LUMO to HOMO is pictured in Fig. 3, and the orbital mode of the transition is defined as π feature to π^* feature, which is a permissible electronic transition generally. Upon photoexcitation, the electron density on O1 atom decreases whereas that on N3 atom is increases, which is conducive to the proton shift from O1 atom to N3 atom in excited state. Furthermore, the polarity of the solvent environment also plays vital roles on the spectroscopic properties. Thus, along with the solvent electrostatic constant decreases, at the same time, the energy gap between the HOMO and LUMO exhibits intensive dependence on the solvent electrostatic constant, namely in case of the solvent electrostatic constant gradually declines and the energy gap becomes the smaller. As a consequence, a bathochromic shift could be observed in the wavelengths of absorption and fluorescence spectra (Figs. S3–S5 in Supporting information). Therefore, the analysis of FMOs essentially elucidates that the enhancement of intramolecular hydrogen bond is ascribed to the electron density rearrangement upon photo-induction, which undermines the electronegativity of the original proton donor atoms, accordingly giving the driving force to proceed the hydrogen protons transfer to the neighboring proton acceptors.

Aiming to respectively investigate the excitation mode for the normal and tautomeric form of MHBT, we calculated the FMOs characteristics in the electronic transition using PBE0 method. Simultaneously, B3LYP method were utilized as well to compare with the PBE0 calculation results at the same level. As shown in Fig. S6 (Supporting information), the results uncover that a proton-coupled electron transfer process occurred in the S_1 state, which is similar to the situation we calculated in both the theoretical levels. Although a minor difference is observed in the calculated emission energy by using the PBE0 and the B3LYP method, it can be rationalized by the Hartree-Fork exchange of different percentage between the PBE0 and B3LYP functional.

After the FMOs are calculated, the PECs of molecule MHBT in these four organic solvents are further constructed. It is worth noting the PECs are a kind of function of the single-point energy and the length of hydrogen bond, which can uncover the accessibility of the ESIPT process more vividly and intuitively [37–39]. As displayed in Fig. S7 (Supporting information), the energy barriers of molecule MHBT tend to overcome to proceed proton shift in the S_1 state are 2.196 kcal/mol (DMSO), 2.203 kcal/mol (ACN), 2.246 kcal/mol (DCM) and 2.397 kcal/mol (DIO), respectively. Note that this does correspond to the previous theoretical outcome that the ESIPT is more favorable while the solvent dielectric constant gradual declines. By contrast, the energy barrier of proton transfer in the S_0 state are 7.135 kcal/mol (DMSO), 7.154 kcal/mol (ACN), 7.310 kcal/mol (DCM) and 8.170 kcal/mol (DIO), respectively, indicating that proton transfer process is not prone to take place and progress in S_0 state. However, the other way around, the reverse proton shift in the keto form can be allowed with minimal energy barrier in the S_0 state: 1.305 kcal/mol (DMSO), 1.707 kcal/mol (ACN), 2.071 kcal/mol (DCM) and 2.497 kcal/mol (DIO), respectively (Fig S8 in Supporting information). In other words, this makes sure that relaxed tautomeric MHBT can get back to the normal form in S_0 state, which is also termed "ground-state proton transfer". Meanwhile, it is noted that the calculation of IRCs also prompted that the enol form as well as keto form involved can be properly integrated into the overall ESIPT process through the corresponding TS structures (Fig. S12 in Supporting information). Given such a four-level energy cycle (Scheme 1b), the ESIPT process is proven to be allowed in molecule MHBT. It is worth mentioning that, as exhibited in Table S5 (Supporting information), the single point energy of Enol, Keto and TS forms for molecule MHBT were also proved that above mentioned viewpoint, and they are closely related to the dielectric constant of the solvent as well.

On the other hand, the PECs as a function of dihedral angle could be utilized to essentially illustrate twisted intramolecular charge transfer state (TICT) process as well. Especially in MHBT, four substituted phenyl rings including the benzothiazole moiety are connected to an imidazole core *via* the carbon-carbon bonds, forming a similar rotor-like structure, in which the imidazole-core acts as a stator. Generally, the MHBT may exist in some twisted conformation along the single bonds to reach local minimum point of the relative energy. As displayed in Table S4 (Supporting information), the dihedral angle θ_1 hardly changes in S_0 and S_1 states with large energy barrier and it remains nearly planar whatever the dielectric constant of solvents decreases, because of the conducive process of ESIPT. By contrast, these dihedral angles of θ_2, θ_3, θ_4 and θ_5 showed torsion in different degrees after photoexcitation. Significantly, a substantial differentiation is observed in the PECs as a function of θ_4, as presented in Fig. S9 (Supporting information). Namely, the energy barrier is relatively bigger in the vertical angle (90°) in S_0 state, while in S_1 state the energy barrier is smaller and easier to cross. This therefore demonstrates that it tends to be thermally stable and more favorable structure in the excited state. The results may be rationalized by the TICT process in which a near-perpendicular conformation is given owing to the rotational motion of the electron-acceptor group and/or the electron-donor moiety, simultaneously alonged with the ICT process. Finally, it also contributes to the dark state of molecule MHBT in solution whereas inhibiting it can restore the fluorescence emission, especially by inducing aggregation. Thus, in such cases, the cooperative and synergistic actions of the twisted conformations and the restricted intramolecular rotations (RIR) which debilitates the undesirable intermolecular $\pi-\pi$ stacking may contribute to the AIE phenomenon. So, AIE experiments for molecule MHBT are conducted in THF/*n*-hexane and CH_3OH/H_2O solvent systems, respectively (Figs. S10 and S11 in Supporting information).

According to our previous works [33], the counter-absorption and emission spectrum of molecule MHBT have been measured, as shown in Fig. S3. Furthermore, the calculated absorbance and fluorescence spectra of molecule MHBT as well using the same functional and basis set of PBE0/6-31G(d, p) in four kinds of organic solvents, and the results we obtained is consistent with that acquired by the experimental values (Fig. S3). This finding again val-

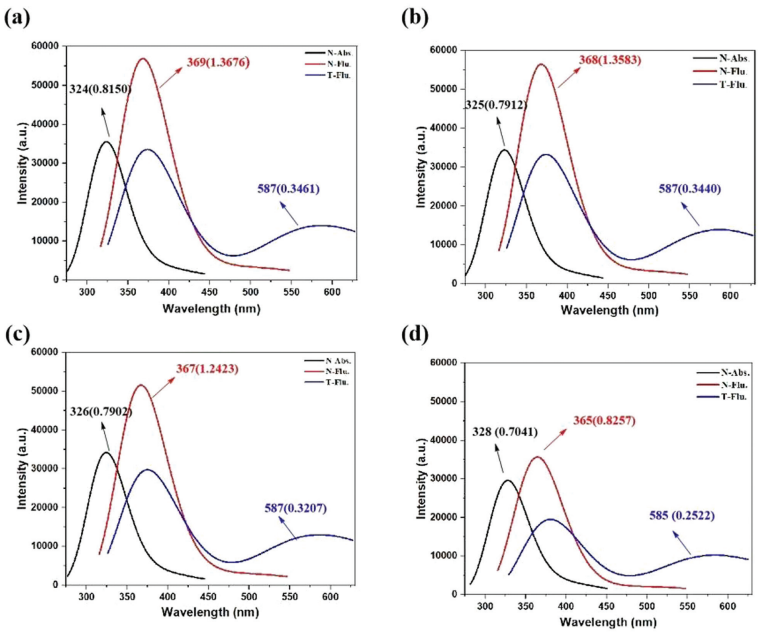

Fig. 4. The calculated absorption and fluorescence spectrum of molecule MHBT in four kinds of organic solvent (a) DMSO, (b) ACN, (c) DCM and (d) DIO, respectively. Abs.: absorption; Flu.: fluorescence; N and T represent normal form and tautomer form, respectively.

idated that the calculation method using in this study are rational and reliable. The schematic illustrative of the theoretical absorption and fluorescence spectra were illustrated in Fig. 4, which authenticates our calculation results. As shown in Fig. 4, the calculated values of maximum absorbance spectrum are: DMSO (324 nm), ACN (325 nm), DCM (326 nm) and DIO (328 nm), the corresponding calculate values of emission spectra for enol form and keto form are 369 nm and 587 nm (DMSO), 368 nm and 587 nm (ACN), 367 nm and 587 nm (DCM), 365 nm and 585 nm (DIO), respectively. Hence, the Stokes shift of molecule MHBT in enol form in these four solvents are 45 nm, 43 nm, 41 nm and 37 nm, respectively, and the Stokes shift of molecule MHBT in keto form are 263 nm, 262 nm, 261 nm, and 257 nm, respectively. Obviously, the reducing order of Stokes shift with a decrease in dielectric constant solvent. Most worthy of mention is that this fact seems to exist in both enol and keto forms. Therefore, we can discover that the Stokes shift of fluorescence for keto forms is larger than that in enol forms, which further demonstrates that the hydrogen proton shift process does a great influence on the photophysical chemical properties of the molecule MHBT. Meanwhile, we also noticed that the strength of the theoretically calculated absorption or fluorescence peak reduces as the polarity of the solvent decreases, which may be attributed to greater charge transfer character.

Herein, we have comprehensively elucidated the existence of cooperative mechanisms of molecule MHBT in a theoretical way by using DFT and TD-DFT methods. Above all, the stable conformations of the different electronic states for molecule MHBT in different solvent environments were optimized. From the analysis of the change of the bond angle, bond length, electron hole, MEP, RDG scatter diagrams and IR vibration spectra and then discover that the obvious solvent dependence of the intramolecular hydrogen bond (H2···O1) in the S_1 state. The lower the dielectric constant of the organic solvent, the intensity of the intramolecular hydrogen bond become stronger. Note that the calculated outcomes of FMOs indicated that the ICT effect could facilitate the ESIPT process, in which a larger electronic transition energies may lead to a larger bathochromic shift in absorbance and fluorescence spectrum. Additionally, the PECs of the single bond rotation and dihedral angle were evaluated to rationalize the RIR process, a crucial characteristic of AIE effect. By the theoretical calculation, the reasonable interplay of ESIPT, ICT and AIE in molecule MHBT is skillfully explained. The rotor-like structure, intramolecular hydrogen-bond and the interaction of electron-donating and electron-withdrawing units in molecule MHBT contribute cooperatively to the synergetic effect of these three working mechanisms. Hence, our calculations provide a detailed ground and excited state picture of AIE-ESIPT fluorophore MHBT, and the revealed mechanism is expected to be further applied to develop specific fluorescent probes to meet the needs of biomedical applications.

Declaration of competing interest

The authors declare that they have no known competing financial interests or personal relationships that could have appeared to influence the work reported in this paper.

Acknowledgments

W. Zeng sincerely thank the financial contribution from the National Natural Science Foundation of China (Nos. 81971678 and 81671756), M. Liu appreciate the Natural Science Foundation of Hunan Province (No. 2021JJ41008) and the Key Project of Changsha Science and Technology Plan (No. kh2201059) for financial support.

Supplementary materials

Supplementary material associated with this article can be found, in the online version, at doi:10.1016/j.cclet.2022.107940.

References

[1] Z. Pode, R. Peri-Naor, J.M. Georgeson, et al., Nat. Nanotechnol. 12 (2017) 1161–1168.
[2] C. Yan, Y. Zhang, Z. Guo, Coord. Chem. Rev. 427 (2021) 213556.
[3] X. Wu, W. Shi, X. Li, H. Ma, Acc. Chem. Res. 52 (2019) 1892–1904.
[4] J. Ma, W. Li, J. Li, et al., Talanta 182 (2018) 464–469.
[5] W. Chen, X. Ma, H. Chen, S.H. Liu, J. Yin, Coord. Chem. Rev. 427 (2021) 213584.
[6] X. Tian, T. Liu, Y. Ma, et al., Angew. Chem. Int. Ed. 60 (2021) 24566–24572.
[7] V.S. Padalkar, S. Seki, Chem. Soc. Rev. 45 (2016) 169–202.
[8] S. Goswami, A. Manna, S. Paul, et al., Chem. Commun. 49 (2013) 2912–2914.
[9] X. Cheng, S. Huang, Q. Lei, et al., Chin. Chem. Lett. 33 (2022) 1861–1864.

[10] B. Feng, Y.L. Zhu, J.X. Wu, et al., Chin. Chem. Lett. 32 (2021) 3057–3060.
[11] B. Valeur, I. Leray, Coord. Chem. Rev. 205 (2000) 3–40.
[12] K. Komatsu, Y. Urano, H. Kojima, T. Nagano, J. Am. Chem. Soc. 129 (2007) 13447–13454.
[13] X. Li, S. Zhang, J. Cao, et al., Chem. Commun. 49 (2013) 8656–8658.
[14] M.J. Chang, C.X. Yan, L. Shi, et al., Chin. Chem. Lett. 33 (2022) 762–766.
[15] M.Z. Zuo, W.R. Qian, M. Hao, et al., Chin. Chem. Lett. 32 (2021) 1381–1384.
[16] X. Cai, B. Liu, Angew. Chem. Int. Ed. 59 (2020) 9868–9886.
[17] W. He, T. Zhang, H. Bai, et al., Adv. Healthc. Mater. (2021) 2101055.
[18] K. Li, G. Cheng, C. Ma, et al., Chem. Sci. 4 (2013) 2630–2644.
[19] S. Zhang, W. Li, L. Yao, et al., Chem. Commun. 49 (2013) 11302–11304.
[20] Y.M.A. Yamada, S.M. Sarkar, Y. Uozumi, J. Am. Chem. Soc. 134 (2012) 3190–3198.
[21] G.X. Zhu, Z.C. Duan, H.Y. Zhu, et al., Chin. Chem. Lett. 33 (2022) 266–270.
[22] S. Zhang, L. Yao, Q. Peng, et al., Adv. Funct. Mater. 25 (2015) 1755–1762.
[23] Y.S. Zhao, H. Fu, A. Peng, et al., Acc. Chem. Res. 43 (2010) 409–418.
[24] G.L. Gao, Y.R. Jia, H. Jiang, M. Xia, Dyes Pigm. 186 (2021) 109030.
[25] W. Li, D. Liu, F. Shen, et al., Adv. Funct. Mater. 22 (2012) 2797–2803.
[26] R. Visbal, M.C. Gimeno, Chem. Soc. Rev. 43 (2014) 3551–3574.
[27] G. Gajeles, S.H. Lee, Eur. Polym. J. 120 (2019) 109240.
[28] B.S. Kim, J.Y. Lee, Adv. Funct. Mater. 24 (2014) 3970–3977.
[29] T. Gao, H. Zeng, H. Xu, et al., Theranostics 8 (2018) 1911–1922.
[30] S. Huang, T. Gao, A. Bi, et al., Dyes Pigm. 172 (2020) 107830.
[31] T. Gao, S. Yang, X. Cao, et al., Anal. Chem. 89 (2017) 10085–10093.
[32] T. Gao, S. Wang, W. Lv, et al., Chem. Commun. 54 (2018) 3578–3581.
[33] M. Liu, R. Xiao, B. Feng, et al., Sens. Actuator. B 342 (2021) 130038.
[34] G.J. Zhao, K.L. Han, J. Chem. Phys. 127 (2007) 024306.
[35] J. Zhao, J. Chen, Y. Cui, et al., Phys. Chem. Chem. Phys. 17 (2015) 1142–1150.
[36] W.Q. Deng, L. Sun, J.D. Huang, et al., Nat. Protoc. 10 (2015) 632–642.
[37] Z. Tang, Y. Qi, Y. Wang, et al., J. Phys. Chem. B 122 (2018) 3988–3995.
[38] Y. Qi, Z. Tang, H. Zhan, et al., Spectrochim. Acta Part A: Mol. Biomol. Spectrosc. 224 (2020) 117359.
[39] X. Wang, Y. Li, P. Song, F. Ma, Y. Yang, Phys. Chem. Chem. Phys. 22 (2020) 6391–6400.